

Measuring the Hubble constant with black sirens

Hebertt Leandro,¹ Valerio Marra^{2,3,4} and Riccardo Sturani⁵

¹*Departamento de Física Teórica e Experimental, Universidade Federal do Rio Grande do Norte, Natal-RN, Brazil*

²*Núcleo de Astrofísica e Cosmologia & Departamento de Física, Universidade Federal do Espírito Santo, 29075-910, Vitória, ES, Brazil*

³*INAF – Osservatorio Astronomico di Trieste, via Tiepolo 11, 34131, Trieste, Italy*

⁴*IFPU – Institute for Fundamental Physics of the Universe, via Beirut 2, 34151, Trieste, Italy*

⁵*International Institute of Physics, Universidade Federal do Rio Grande do Norte, Natal-RN, Brazil*

Accepted XXX. Received YYY; in original form ZZZ

ABSTRACT

We investigate a recently proposed method for measuring the Hubble constant from gravitational wave detections of binary black hole coalescences without electromagnetic counterparts. In the absence of a direct redshift measurement, the missing information on the left-hand side of the Hubble-Lemaître law is provided by the statistical knowledge on the redshift distribution of sources. We assume that source distribution in redshift depends on just one unknown hyper-parameter, modeling our ignorance of the astrophysical binary black hole distribution. With tens of thousands of these “black sirens” – a realistic figure for the third generation detectors Einstein Telescope and Cosmic Explorer – an observational constraint on the value of the Hubble parameter at percent level can be obtained. This method has the advantage of not relying on electromagnetic counterparts, which accompany a very small fraction of gravitational wave detections, nor on often unavailable or incomplete galaxy catalogs.

Key words: gravitational waves–black hole mergers–cosmological parameters

1 INTRODUCTION

The Hubble constant H_0 – the current expansion rate of space – is a fundamental parameter that sets the time and distance scales of the observable universe. It is then alarming that the local model-independent determination of the Hubble constant via calibrated local Type Ia supernovae (Riess et al. 2021) is in strong tension with the CMB determination based on the standard Λ CDM model of cosmology (Aghanim et al. 2020). The tension reached 4.5σ (Camarena & Marra 2021) and it could very well signal the need of a new standard model of cosmology (Knox & Millea 2020). The possibility of physics beyond Λ CDM has been urging the scientific community to measure H_0 via the widest range possible of probes and techniques: besides Cepheids, strong lensing time delays, tip of the red giant branch, megamasers, Oxygen-rich Miras and surface brightness fluctuations (see Verde et al. 2019; Di Valentino et al. 2021; Perivolaropoulos & Skara 2021; Khetan et al. 2021, for details).

Gravitational wave (GW) observations are expected to play an important role in the determination of H_0 already in the near future (Gray et al. 2020), thanks first to the second generation detectors LIGO (Aasi et al. 2015), Virgo (Acernese et al. 2015) and KAGRA (Akutsu et al. 2020), and then to the third generation detectors Einstein Telescope (Punturo et al. 2010) and Cosmic Explorer (Abbott et al. 2017a). The reason is twofold. First, GW observations are a new and powerful probe so that an independent and precise measurement of H_0 will be obtained. Second, GW observations already with second generation detectors will cover the most interesting

redshift range ($0.2 \lesssim z \lesssim 0.7$, Abbott et al. 2020) as far as the Hubble tension is concerned. It is low-enough so as to be considered “late universe” but high enough so that local inhomogeneities are not supposed to have any impact via the so-called cosmic variance on H_0 (Camarena & Marra 2018). In other words, GW observations have the potential to shine light in a definitive way on the tension between early- and late-universe measurements of H_0 .

So far, different technics, not mutually exclusive, have been used, all exploiting the fact that compact binary coalescences are *standard sirens* (Schutz 1986; Holz & Hughes 2005). If an electromagnetic counterpart is available, then one can break the intrinsic degeneracy between H_0 and the coalescence redshift z and precisely determine the Hubble constant with just a few tens of events (Chen et al. 2018).¹ The first, and so far unique, of these standard sirens was GW170817 and provided alone a 14% measurement of H_0 (Abbott et al. 2017b). On the other hand, most of the observed binary coalescences do not have electromagnetic counterparts and the redshifts of galaxies in the angular position of the coalescence, inferred from galaxy catalogs, can be used to break the H_0 - z degeneracy (see Schutz 1986 and the recent Diaz & Mukherjee 2021). The first of these *dark sirens* was GW170814 (Soares-Santos et al. 2019). Although not yet constraining, given the rapidly increasing number of detections, one expects percentage level constraints after 50 events (Del Pozzo 2012), if catalogs are

¹ See also Dalal et al. (2006); Nissanke et al. (2010) for the role of gamma-ray bursts in conjunction with standard sirens.

complete enough (see also [Zhu et al. 2021](#)). Confining oneself to the binary neutron star case, observation of tidal effects can break the gravitational mass-redshift degeneracy, enabling the reconstruction of the Hubble relations without electromagnetic counterparts ([Messenger & Read 2012](#)). Alternatively, one can exploit the spatial clustering scale between galaxies and gravitational wave sources, as proposed by [Mukherjee & Wandelt \(2018\)](#); [Mukherjee et al. \(2021a,b\)](#): this method is expected to produce accurate and precise measurements of the expansion history of the universe.

Finally, another intriguing method uses the expected gap in the black hole mass function due to the pair-instability supernovae ([Heger et al. 2003](#)). Features in the mass distribution break indeed the mass-redshift degeneracy intrinsic to GW observations, so that it is possible to measure H_0 without electromagnetic counterparts or host galaxy catalogs ([Farr et al. 2019](#); [Ezquiaga & Holz 2021](#); [You et al. 2021](#); [Mastrogiovanni et al. 2021](#)).

Here, improving on the idea presented in [Ding et al. \(2019\)](#), we propose an alternative method to measure the Hubble constant. This technique uses all observed binary black hole coalescences, which represent the quasi totality of the events: the H_0 - z degeneracy of these *black sirens* is broken via the expected (parameter-dependent) redshift distribution of coalescences.² As we will argue, instead of using galaxy catalogs, unavailable or incomplete for most events, one can exploit the prior distribution of the coalescence redshift, suitably convolved with the instrumental sensitivity of the detectors. In particular, our method is expected to outperform methods that rely on galaxy catalogs in the limit of many observations ($O(10^4)$) with poor localization at $z \sim 1 - 2$. Therefore, it could be tested with coalescences observed by second generation detectors during their future runs and it should definitely be efficient with third generation detectors.

This paper is organized as follows: Section 2 presents the method, whose limiting cases are treated analytically and discussed in Section 3. The forecasted results relative to third generation detectors are presented in Section 4. We conclude in Section 5.

2 METHOD

Throughout this paper we will adopt the standard model of cosmology, according to which the universe is spatially flat and has an energy content made of vacuum energy (the cosmological constant Λ) and pressureless matter (mostly cold dark matter, CDM). The low-redshift background evolution of the flat Λ CDM model is completely specified by the values of the Hubble constant H_0 and of the matter density parameter Ω_m . In particular, in our model, the luminosity distance is related to the redshift via:

$$d_L^{(t)}(z) = \frac{c(1+z)}{H_0} \int_0^z \frac{d\bar{z}}{E(\bar{z})}, \quad (1)$$

$$E(z) \equiv \frac{H(z)}{H_0} = \sqrt{\Omega_m(1+z)^3 + 1 - \Omega_m}, \quad (2)$$

with the comoving distance $d_C^{(t)} = d_L^{(t)}/(1+z)$, with the index (t) standing for “theoretical”.

² See also [Ye & Fishbach \(2021\)](#) for a similar idea using binary neutron stars only.

Let us now consider one coalescence event. GW detections measure the luminosity distance d_L so that one can build the posterior distribution f of the cosmological parameters and binary black hole (BBH) redshift as follows:

$$f(H_0, \Omega_m, z|d_L) = \frac{p_{\text{tot}}(H_0, \Omega_m, z) \mathcal{L}(d_L, |H_0, \Omega_m, z)}{\mathcal{E}}, \quad (3)$$

where here the evidence \mathcal{E} is just a normalization constant. We will now discuss the prior p_{tot} and the likelihood \mathcal{L} .

2.1 Prior

Using the product rule, the prior can be written as:

$$p_{\text{tot}}(H_0, \Omega_m, z) = p(H_0) p(\Omega_m) p(z|H_0, \Omega_m). \quad (4)$$

We assumed that Ω_m and H_0 are independent because for the former we use an informative prior from Supernovae Ia, which is independent from H_0 . We adopt the almost Gaussian prior from the Pantheon dataset ([Scolnic et al. 2018](#)):

$$p(\Omega_m) \propto \exp \left[-\frac{(\Omega_m - \Omega_m^p)^2}{2\sigma_{m,p}^2} \right], \quad (5)$$

where of $\Omega_m^p = 0.298$ and $\sigma_{m,p} = 0.022$.

Regarding $p(H_0)$, as we aim at measuring the Hubble constant with black sirens, we adopt a flat broad prior:

$$p(H_0) \propto \begin{cases} \text{const} & \text{if } H_0 \in [20, 140] \text{ km s}^{-1} \text{Mpc}^{-1} \\ 0 & \text{otherwise} \end{cases}, \quad (6)$$

which is the same prior adopted by [Soares-Santos et al. \(2019\)](#).

The prior on the observed coalescence redshift $p(z|H_0, \Omega_m)$ is the nontrivial piece of information necessary to extract information on H_0 from gravitational wave observations. The standard dark-siren approach estimates the redshift prior via a galaxy catalog that covers the sky localization of the event ([Soares-Santos et al. 2019](#); [Fishbach et al. 2019](#); [Abbott et al. 2021a](#)). This approach has the advantage of correlating the coalescence to the actual nearby galaxies and, in particular, to their large-scale structure of voids, filaments and clusters. However, the galaxy catalog may be incomplete or unavailable. The idea at the base of our black-siren method is to estimate $p(z|H_0, \Omega_m)$ theoretically. More precisely, in the present paper we will obtain the redshift prior via an analytical estimation of the star-formation rate, convolved with a suitable star-formation to binary coalescence delay, while we leave for future work the use of synthetic galaxy catalogs from state-of-the-art hydrodynamical simulations.

We model the redshift prior via two contributions:

$$p(z|H_0, \Omega_m) = A(H_0, \Omega_m) R_m(z) f_C \left(d_C^{(t)}(z) \right), \quad (7)$$

which we now explain in details. In the previous equation A is a normalization constant which may depend on all the parameters but z .

2.1.1 Merger rate

The first contribution $R_m(z)$ is the rate number (N_m) density of mergers in the detector frame (number of mergers per detector time per redshift) which will be expressed as:

$$R_m^{(\tau)}(z) \equiv \frac{dN_m^{(\tau)}}{dt_d dz}, \quad (8)$$

where we omit the inconsequential normalization constant and the hyperparameter τ is discussed below. Following Vitale et al. (2019); Soares De Souza & Sturani (2021), we model R_m via the total merger rate per comoving volume in the source frame $\mathcal{R}_m^{(\tau)} \equiv \frac{dN_m^{(\tau)}}{dV dt_s}$:

$$R_m^{(\tau)}(z) = \frac{1}{1+z} \frac{dV}{dz} \mathcal{R}_m^{(\tau)}(z), \quad (9)$$

where the $1+z$ term in the denominator arises from converting source-frame time t_s to detector-frame time t_d , and dV/dz is the cosmology-dependent comoving volume element per unit redshift interval:

$$\frac{dV}{dz} = \frac{4\pi}{H(z)} \frac{c d_L^2(z)}{(1+z)^2} = \frac{4\pi}{E(z)} \left(\frac{c}{H_0}\right)^3 \left[\int_0^z \frac{d\bar{z}}{E(\bar{z})}\right]^2. \quad (10)$$

Then, we model $\mathcal{R}_m^{(\tau)}$ via a delayed volumetric BBH formation rate \mathcal{R}_f . Specifically, we account for the stochastic delay between star formation and BBH merger via a Poissonian distribution of characteristic delay τ :

$$\mathcal{R}_m^{(\tau)}(z) = \frac{1}{\tau} \int_z^\infty dz_f \frac{dt}{dz_f} \mathcal{R}_f(z_f) \exp\left[-\frac{t(z_f) - t(z)}{\tau}\right], \quad (11)$$

where

$$t(z) \equiv \frac{1}{H_0} \int_0^z \frac{d\bar{z}}{(1+\bar{z})E(\bar{z})} \quad (12)$$

is the time spent between redshift z and the present epoch. Note that $\mathcal{R}_m^{(\tau)}$ depends on τ only via the dimension-less combination $H_0\tau$.

Finally, we assume that the BBH volumetric formation rate is proportional to the star formation rate density $\psi(z)$ at the same redshift:

$$\mathcal{R}_f(z_f) \equiv \frac{dN_f}{dV dt_f} \propto \psi(z_f). \quad (13)$$

In other words we are not considering the time between star formation and BBH formation, which should be negligible given the time scale of BBH coalescence. We adopt the measured star formation rate from Madau & Dickinson (2014):

$$\psi_{\text{MD14}}(z) = 0.015 \frac{(1+z)^{2.7}}{1 + \left(\frac{1+z}{C}\right)^{5.6}} M_\odot \text{ yr}^{-1} \text{ Mpc}^{-3}, \quad (14)$$

with $C = 2.9$. This star formation rate may not correspond to the one realized in nature. In the Appendix A we show that the addition of another hyperparameter can absorb the effect of a different star formation rate and produce an unbiased determination of the Hubble constant.

As said earlier, the characteristic delay τ is a hyperparameter of the redshift prior. We adopt a flat hyperprior:

$$p(\tau) \propto \begin{cases} \text{const} & \text{if } \tau \in [100 \text{ Myr}, t_0(H_0, \Omega_m)] \\ 0 & \text{otherwise} \end{cases}, \quad (15)$$

where t_0 is the age of the universe (since we observe the coalescence it must be $\tau < t_0$). One can then consider the following compound distribution as the coalescence prior:

$$R_m(z) = \int_0^\infty d\tau p(\tau) R_m^\tau(z). \quad (16)$$

Note that, numerically, it is equivalent to include τ as a nuisance parameter with prior $p(\tau)$. We will adopt this point of view when considering a generic number n of events.

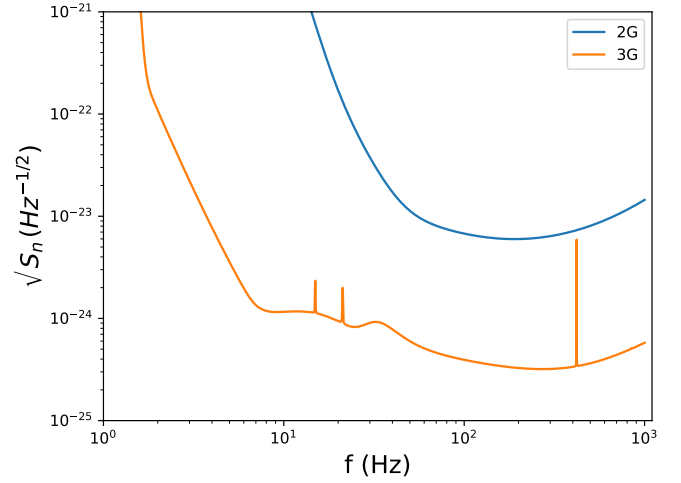


Figure 1. Second and third generation spectral noise densities. The 2G noise curve has been obtained by a fit to the LIGO Hanford O3 data around the event GW190814 based on the “Zero Detuning High Power” spectral noise density implemented in LALSuite (LIGO Scientific Collaboration 2018). For the 3G curve we adopted the noise spectral density “D” from Hall & Evans (2019).

2.1.2 Detector sensitivity

The last piece in Eq. (7), $f_C(d_C^{(t)})$, models the LIGO-Virgo detector sensitivity on the luminosity distance: obviously more distant sources are less likely to be detected than nearer ones. Indeed, coalescences are observed if a signal-to-noise ratio (SNR) larger than 8 is achieved. The SNR is computed by comparing the f -domain waveform $\tilde{h}(f)$ with the detector noise S_n :

$$SNR = 2 \left[\int_0^\infty df \frac{|\tilde{h}(f)|^2}{S_n(f)} \right]^{1/2}, \quad (17)$$

$$\tilde{h}(f) = F_+ \tilde{h}_+(f) + F_\times \tilde{h}_\times(f), \quad (18)$$

where the pattern functions $F_{+,\times}$ are function of the two angles locating the source in the sky (α, δ) and the polarization angle ψ , and the GW polarizations $\tilde{h}_{+,\times}$ are given at leading order (quadrupole formula) by:³

$$\tilde{h}_+ = \left(\frac{5}{24}\right)^{1/2} \frac{\pi^{-2/3}}{d_L^{(t)}} \mathcal{M}_c^{5/6} f^{-7/6} \left(\frac{1 + \cos^2 \iota}{2}\right)^2 e^{i\phi(f)}, \quad (19)$$

$$\tilde{h}_\times = \left(\frac{5}{24}\right)^{1/2} \frac{\pi^{-2/3}}{d_L^{(t)}} \mathcal{M}_c^{5/6} f^{-7/6} \cos \iota e^{i\phi(f) + i\pi/2}, \quad (20)$$

which depend on the luminosity distance, the orientation ι and the redshifted chirp mass $\mathcal{M}_c \equiv M_c(1+z)$. The chirp mass is $M_c \equiv \eta^{3/5} M$, where $M \equiv m_1 + m_2$, $\eta \equiv m_1 m_2 / M^2$, and m_i are the individual constituent masses. The angle ι gives the relative orientation between the binary orbital plane and the observation direction. Fig. 1 shows the square root of the noise spectral density $\sqrt{S_n}$ used to estimate the SNR for second (2G) and third (3G) generation detectors.

To relate the astrophysical to the *detected* merger rate one needs to take into account selection effect, i.e. to estimate

³ Note that the interference term between \tilde{h}_+ and \tilde{h}_\times vanishes in the SNR integral.

Table 1. Parameter space that is uniformly explored (except for masses) to sample the SNR of Eq. (17). For the individual masses the distribution adopted is a broken power law $\propto m_i^{-1.5}$ (m_i^{-5}) for $m_i < 40M_\odot$ ($40 < m_i/M_\odot < 80$) for solar mass black holes and a log prior for intermediate masses $120 < M/M_\odot < 10^4$.

Parameter	Quantity	Interval
Comoving distance	$d_C^{(t)}/\text{Mpc}$	$[100, 1.2 \cdot 10^4]$
Individual mass	m_i/M_\odot	$[1.2, 10^4]$
Mass ratio	$q = m_2/m_1$	$> 10^{-3}$
Binary orientation	$\cos \iota$	$[-1, 1]$
Polarization	ψ	$[0, 2\pi]$
Right ascension	α	$[0, 2\pi]$
Declination	δ	$[0, \pi]$

how likely it is to detect a source located at a given distance from the observatory, which is obtained by averaging over the source parameters to get the average distribution of detections as a function of distance. The requirement for detection is that the signal has $SNR \geq 8$, and averaging is performed over masses and angles as reported in Table 1.

The astrophysical mass distribution of stellar-mass black holes can be inferred from LIGO/Virgo O1, O2, O3a data as described in Abbott et al. (2019, 2021b). This is relevant for 2G detectors as they are sensitive to binaries with total mass up to $\sim O(100M_\odot)$. We can assume that the mass of the heavier binary component is distributed according to a broken power law with exponents $\alpha_1 = -1.5$ and $\alpha_2 = -5$ for masses between 5 and $60 M_\odot$, with the slope change occurring at $m_{\text{break}} = 40M_\odot$. The mass ratio q is assumed to be distributed according to $p(q) \propto q^{-1}$ with $0.1 \leq q \leq 1$, with a lower cutoff on the lighter mass assuming $1.2M_\odot < m_2$. Third generation detectors will be also sensitive to intermediate-mass black holes with $m_i \gtrsim 10^2 M_\odot$. As their distribution is completely unknown, we have assumed a mass gap from 80 to $120M_\odot$ due to pair-instability supernovae (Heger et al. 2003) and an uninformative d log prior up to $m_i < 10^4 M_\odot$. In the same spirit of the 2G case, that is to use a concrete example to test the method, we assume the distribution of the primary mass to be $\propto 1/m_1$ for $120 \leq m_1/M_\odot \leq 10^4$ and for the mass ratio in this region the prior $p(q) \propto q^{1/2}$.

It is important to stress that stellar- and intermediate-mass black hole population properties are not precisely known and that here we wish to use indicative values for the underlying population to test the efficiency of our method in a realistic case. Moreover, the black hole mass function is only used to evaluate the reach of the detector. Besides this detail, its information is *not* folded into the likelihood to determine cosmological parameters. As we will show, the method proposed here can lead to interesting constraints on H_0 only for a large number of detections $\gtrsim O(10^3)$. Hence, we can safely assume that once accumulating so many detections, the population properties of the sources will be known with great accuracy. The use of a different underlying astrophysical mass distribution will impact both the simulated signals and the priors entering the determination of the H_0 posterior probability distribution, leaving basically unaltered the predictive power of the method.

We use the waveform approximant known as *IMRPhenomD* (Husa et al. 2016; Khan et al. 2016) for spin-less sources generated via LALSuite and noise as in Fig. 1, representative of second and third generation ground-based GW

detectors. After imposing $SNR > 8$ and marginalizing over all parameters but $d_C^{(t)}$, we obtain the distributions $f(d_C^{(t)})$ shown in Fig. 2 whose tail in the 2G and 3G cases can be modeled according to:

$$f_C(d_C^{(t)}) \propto \begin{cases} \exp\left[-\frac{d_C^{(t)}}{d_C^{(\text{cut2})}}\right] & 2\text{G} \\ \exp\left[-\left(\frac{d_C^{(t)}}{d_C^{(\text{cut3})}}\right)^3\right] & 3\text{G} \end{cases}, \quad (21)$$

where $d_C^{(\text{cut2})} = 320$ Mpc and $d_C^{(\text{cut3})} = 7.9$ Gpc.

The decay with the comoving distance is qualitative different in the 2G and 3G cases. In the 2G case, only sources at moderate redshift are visible, as increasing the distance increases the denominator in Eq. (19) thus decreasing the SNR .

In the 3G case, signals with $z > 1$ are visible for a wide range of masses, with the result that the $(1+z)^{5/6}$ dependence at the numerator of Eq. (19) almost cancels the z -dependence of $d_C(1+z)$ at the denominator. As a consequence, the SNR varies approximately according to d_C^{-1} until the redshift pushes the signal to low enough frequencies to fall outside the detector's band, and this happens around $d_C \simeq 12$ Gpc for a wide range of masses, as that is the value at which z steeply increases for small variation of d_C , see Fig. 3.

Note that the SNR depends on the redshifted chirp mass \mathcal{M}_c which depends on redshift. To obtain the simulations presented in Figs. 2 the redshift is not varied independently but instead determined from the distance and the fiducial cosmology (Λ CDM): $z^{\text{fid}} = z(d_C^{(t)}, H_0^{\text{fid}}, \Omega_m^{\text{fid}}) \xrightarrow{z \rightarrow 0} H_0^{\text{fid}} d_C^{(t)}/c$, with $H_0^{\text{fid}} = 69.32 \text{ km s}^{-1} \text{ Mpc}^{-1}$ and $\Omega_m^{\text{fid}} = \Omega_m^p$.

2.2 Likelihood

In the Gaussian approximation, the likelihood can be written according to:

$$\mathcal{L}(d_L, |H_0, \Omega_m, z) \propto \exp\left[-\frac{(d_L - d_L^{(t)}(H_0, \Omega_m, z))^2}{2\sigma_L^2}\right], \quad (22)$$

where to lighten notation the dependence of the likelihood on the luminosity distance uncertainty σ_L has been suppressed.

2.3 Posterior for n coalescences

When combining n coalescences it is convenient to marginalize immediately on the parameters that are specific to a given event so that:

$$f(H_0, \Omega_m, \tau | d_L) \propto p(H_0) p(\Omega_m) p(\tau) \times \int dz p(z | H_0, \Omega_m, \tau) \mathcal{L}(d_L, |H_0, \Omega_m, z), \quad (23)$$

where, as discussed earlier, we treated τ as a nuisance parameter. The expression above can then be generalized to the case of n detections $\{d_{L,i}\}$:

$$f(H_0, \Omega_m, \tau | \{d_{L,i}\}) \propto p(H_0) p(\Omega_m) p(\tau) \times \prod_{i=1}^n \int dz_i p(z_i | H_0, \Omega_m, \tau) \mathcal{L}(d_{L,i} | H_0, \Omega_m, z_i). \quad (24)$$

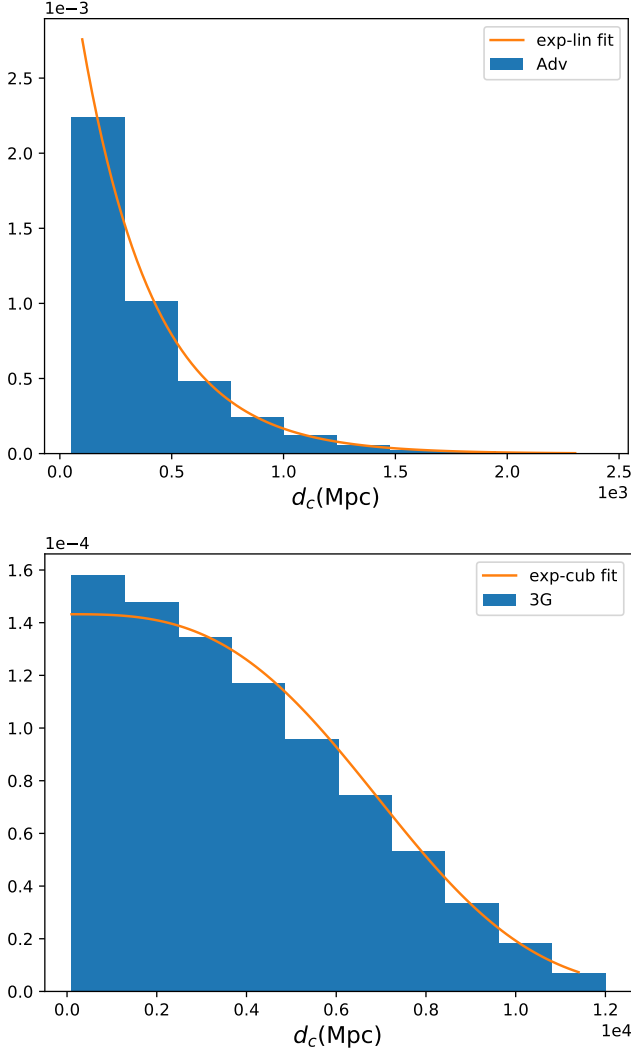


Figure 2. Distribution of the comoving distance d_C for the events satisfying $SNR > 8$, see Eq. (17), averaged over masses and orientations for 2G and 3G detectors. The curve shows the fit of Eq. (21) to the tail of the distribution. Note the different scale for both axis in the two figures.

Numerically, the posterior exploration will be performed on the parameters H_0, Ω_m, τ . In other words, for each point $\{H_0, \Omega_m, \tau\}$ of the parameter space we will estimate the n 1-dimensional integrals of Eq. (24). We parametrize here the inevitable uncertainty in the knowledge of the underlying merger distribution with only one hyperparameter τ , and we address in the Appendix A the issue of the generality of the merger rate function that we adopt in Eq. (16).

3 LIMITING CASES

To understand analytically the statistical inference on H_0 with black sirens it is useful to consider the following limiting cases.

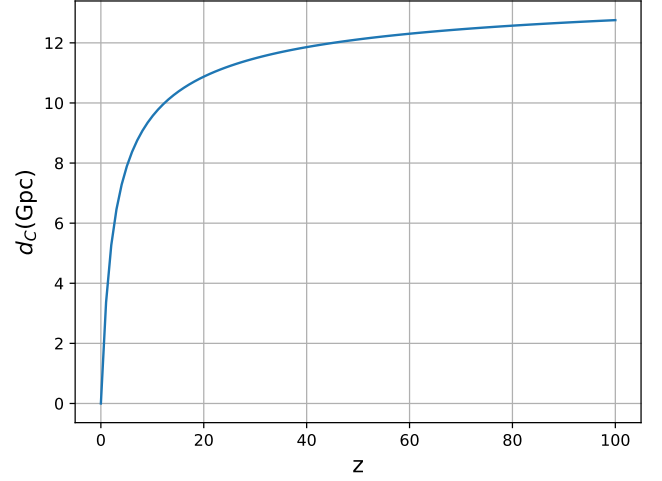


Figure 3. Comoving distance-redshift relationship for standard Λ CDM model.

3.1 Low redshift

It is interesting to take the limit $z \rightarrow 0$ in Eq. (7). First, one has that $\frac{1}{1+z} \frac{dV}{dz} \sim z^2 \sim d_L^2$. Second, from Eq. (14) it follows that $\mathcal{R}_f(z) \sim \text{constant}$ so that, from Eq. (11), one finds that $\mathcal{R}_m^r(z) \sim \text{constant}$. One then finds from Eq. (7) that:

$$p(z|H_0, \Omega_m) \xrightarrow{z \rightarrow 0} d_L^2. \quad (25)$$

In other words, the prior cannot break the H_0 - z degeneracy as it depends just on d_L , which is the quantity measured by GW observations. Equivalently, the information that is able to break the H_0 - z degeneracy comes from a non trivial \mathcal{R}_f .

3.2 Negligible luminosity distance error

Next, we can take the limit $\sigma_L/d_L \rightarrow 0$ in Eq. (24):

$$\begin{aligned} f(H_0, \Omega_m, \tau | \{d_{L,i}\}) &\propto p(H_0) p(\Omega_m) p(\tau) \\ &\times \prod_{i=1}^n \int dz_i A R_m^\tau(z_i) e^{-d_L^{(t)}(z_i)/d_L^{(\text{cut})}} \delta(d_{L,i} - d_L^{(t)}(H_0, \Omega_m, z_i)) \\ &= p(H_0) p(\Omega_m) p(\tau) \prod_{i=1}^n \frac{A R_m^\tau(z_i, H_0, \tau, \Omega_m) e^{-d_{L,i}/d_L^{(\text{cut})}}}{\left| \frac{\partial d_L^{(t)}}{\partial z^{(t)}}(H_0, \Omega_m, z_i) \right|}, \end{aligned} \quad (26)$$

where we used the properties of the Dirac delta function and $z_i = z^{(t)}(d_{L,i}, H_0, \Omega_m)$ is the theoretical redshift associated to $d_{L,i}$ given H_0 and Ω_m , and assumed $f_C = e^{d_L/d_L^{(\text{cut})}}$. We see that, in this limit, the detector sensitivity f_C does not contain cosmological information.

3.3 Infinite number of observations

Statistical inference with black sirens suffers from two sources of uncertainties. The first is due to the uncertainty σ_L on the measurement of the luminosity distance. The second comes from having a finite sample n of observations. Indeed, we are

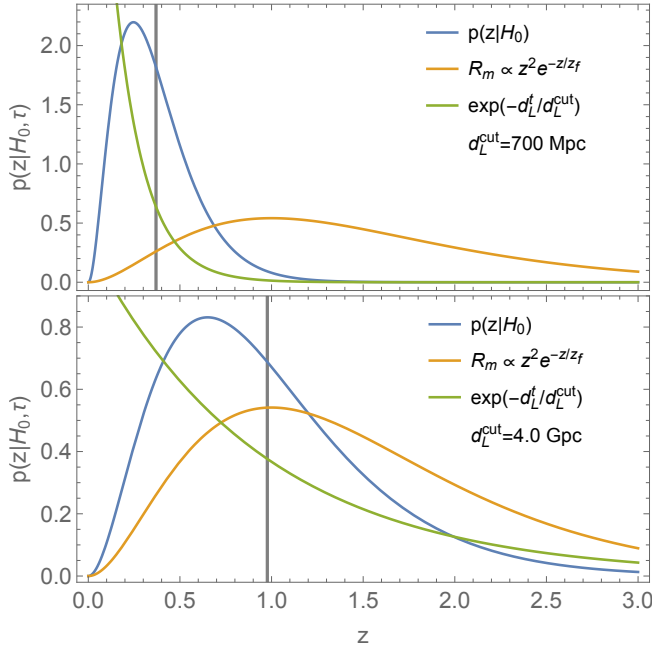


Figure 4. Toy redshift prior of Eq. (28) for $H_0^{\text{fid}} = 70 \text{ km s}^{-1} \text{Mpc}^{-1}$, $z_f = 0.5$ and $d_L^{\text{(cut)}} = 700 \text{ Mpc}$ (top) or $d_L^{\text{(cut)}} = 4.0 \text{ Gpc}$ (bottom). The vertical lines mark the mean redshifts.

constraining parameters to recover the actual distribution of coalescence redshifts.

From Eq. (26) it is easy to see how a fiducial model is recovered in the limit of infinite observations. Assuming flat priors on H_0 , Ω_m and τ :

$$f(H_0, \Omega_m, \tau | \{d_{L,i}\}) \propto \prod_i^n f(d_{L,i} | H_0, \Omega_m, \tau), \quad (27)$$

where $f(d_L^{(t)} | H_0, \Omega_m, \tau)$ is the theoretical distribution in the luminosity distance given the theoretical model (the Jacobian is absorbed by the change of variable). From the previous equation one sees that in the limit $n \rightarrow \infty$ the values of H_0 , Ω_m and τ that maximize the posterior are the ones that were used to produce the measurements $\{d_{L,i}\}$.

3.4 Toy example

To further simplify the analysis we consider the following redshift prior:

$$p(z | H_0) = \left(\frac{c}{H_0 d_L^{\text{(cut)}}} + \frac{1}{z_f} \right)^3 \frac{z^2}{2} e^{-\frac{z}{z_f}} \exp \left(\frac{-c z}{H_0 d_L^{\text{(cut)}}} \right), \quad (28)$$

where we adopted the approximation $d_C^{(t)} \simeq d_L^{(t)} \simeq c z / H_0$, so that we can drop the (anyway weak) dependence on Ω_m . Eq. (28) represents a normalized, reasonable toy model where the factor $z^2 e^{-z/z_f}$ intends to reproduce the astrophysical merger distributions and a detector sensitivity exponentially decaying with redshift has been assumed. Fig. 4 shows this prior for two values of the detector luminosity cut $d_L^{\text{(cut)}}$. The vertical lines mark the mean redshifts $\bar{z} = 3z_f z_c / (z_f + z_c)$, where $z_c(H_0) = H_0 d_L^{\text{(cut)}} / c$.

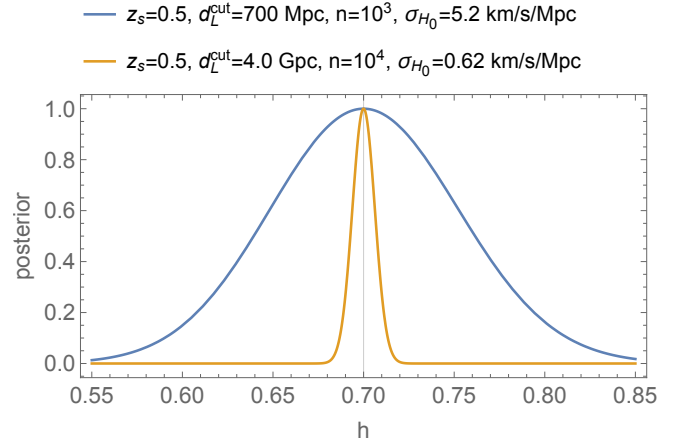


Figure 5. Forecasted constraints on H_0 relative to the toy model of Eq. (29) for a second generation (blue line) and third generation (orange line) detector.

Taking again the limit $\sigma_L/d_L \rightarrow 0$, the posterior becomes:

$$\ln f(H_0 | \{d_{L,i}\}) = 3n \ln \left(\frac{H_0 \bar{d}_L^{\text{(cut)}}}{c z_f} + 1 \right) - n \frac{H_0 \bar{d}_L}{c z_f} \quad (29)$$

$$\stackrel{\text{average}}{=} 3n \left[\ln \left(1 + \frac{H_0 d_L^{\text{(cut)}}}{c z_s} \right) - \frac{H_0 d_L^{\text{(cut)}}}{H_0^{\text{fid}} d_L^{\text{(cut)}} + c z_s} \right],$$

where $\bar{d}_L \equiv \frac{1}{n} \sum_i d_{L,i}$, we omitted additive constants and in the last equation we used:

$$\bar{d}_L = \bar{z} \frac{c}{H_0^{\text{fid}}} = \frac{3z_f z_c (H_0^{\text{fid}})}{z_f + z_c (H_0^{\text{fid}})} \frac{c}{H_0^{\text{fid}}}. \quad (30)$$

The posterior maximum (best fit) is found by solving $\partial \ln f / \partial H_0 = 0$, which gives $H_{0,\text{bf}} = H_0^{\text{fid}}$, that is, the fiducial value of the Hubble constant is recovered in the limit of infinite (infinitely precise) measurements.

Finally, we can compute the Fisher matrix, which, in this case, is just a number:

$$F = - \frac{\partial^2 \ln f(H_0 | \{d_{L,i}\})}{\partial H_0^2} \bigg|_{H_0^{\text{fid}}}, \quad (31)$$

so that:

$$\frac{\sigma_{H_0}}{H_0} = \frac{F^{-1/2}}{H_0} = \frac{1 + z_s/z_c (H_0^{\text{fid}})}{\sqrt{3n}}, \quad (32)$$

which depends on $z_c = H_0^{\text{fid}} d_L^{\text{(cut)}} / c$.

Figure 5 shows the forecasted constraints relative to the toy model of Eq. (29) for a second generation (blue line) and third generation (orange line) detector. This result does not take into account the degeneracy of H_0 with Ω_m and τ . In the next Section we will discuss a realistic forecast.

4 REALISTIC FORECAST

We now perform the full analysis of Eq. (24). The merger rate of Eq. (9) is represented in Fig. 6 for the fiducial values of $\tau = 5 \text{ Gyr}$, $H_0 = 69.32 \text{ km s}^{-1} \text{Mpc}^{-1}$ and $\Omega_m = \Omega_m^{\text{fid}}$, and for the detector sensitivities of 2G and 3G detectors (see Section 2.1.2). We will now consider the case of the future 3G

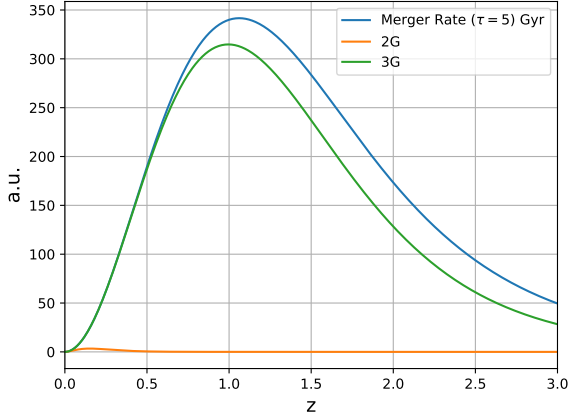


Figure 6. Distribution of detections and merger rate (assuming $\tau = 5$ Gyr). The 2G curve is normalized to unity, the 3G curve and merger rate have normalization consistent with the 2G curve.

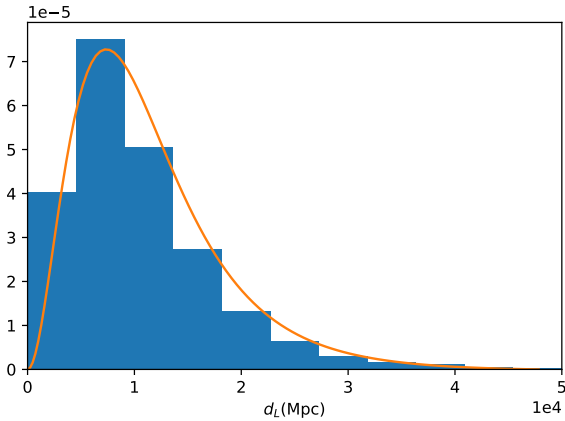


Figure 7. Normalized distribution of simulated detections for a 3G detector.

detectors. Fig. 7 shows the normalized distribution of simulated injections for a 3G detector.

The expected absolute number of binary black hole observations by 3G detectors is poorly constrained because the underlying source distributions is known only to a small extent. By considering very different values of τ and normalizing the local merger rate density at $50 \text{ Gpc}^{-3} \text{ yr}^{-1}$, one can see that, for instance, 10,000 detections can be accumulated in a time varying between a week and few months (Vitale et al. 2019). Here, we consider the following possible scenarios – 10,000, 20,000 and 40,000 detections – which are realistic given the programmed duration of future 3G observation runs.

For the scenario with 10,000 and 20,000 injections, we fully sample the posterior via MCMC using the numerical codes *emcee* (Foreman-Mackey et al. 2013), through its *Bilby* implementation (Ashton et al. 2019), and *getdist* (Lewis 2019). The results are shown in Fig. 8, for the two cases of a 5% and a 10% uncertainty in d_L . We can see that already with 10,000 GW observations it is possible to constrain the Hubble parameter at the few % level.

As can be seen, the maximum of the posterior does not coincide exactly with the fiducial value of the parameters (red

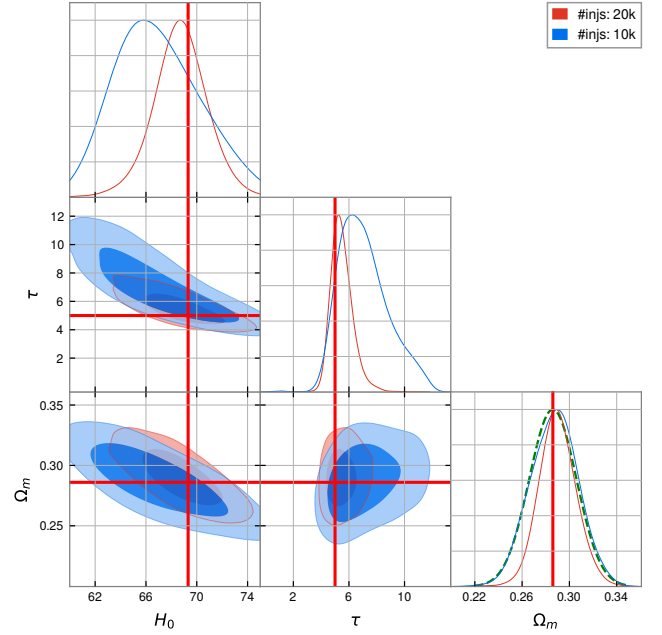


Figure 8. Marginalized constraints on H_0 , τ and Ω_m for 10,000 20,000 simulated injections for the 3G case with 5% relative errors in the measurement of d_L . The fiducial values of the parameters are marked with red lines. The prior on Ω_m is displayed with a green dashed line.

lines in Fig. 8). This is expected because in the present analysis it is not possible to perform a forecast without fluctuations in the observational quantities. Indeed, while one could fix the luminosity distances at their fiducial values, the distribution in redshift of the injections is necessarily stochastic. In other words, here we are considering fully realistic mock datasets.

Then, we analyze the scenario with 40,000 detections via the Fisher matrix approximation, obtained numerically via the *numdifftools* library.⁴ This is necessary because of the increased computational cost: as shown by Eq. (24) one has n numerical integrals for n injections. As explained earlier, the maximum of the posterior randomly walks around the fiducial value of the parameters and, to obtain a more robust estimate of the Fisher matrix against nonlinearities, we consider several sets of injections and average the corresponding Fisher matrices. The result of this procedure is shown in Figure 9 (including also the cases that were analyzed via MCMC) and summarized in Table 2 for the precision and Table 3 for the average bias in the recovered H_0 . The results reported in Fig. 8 give $1-\sigma$ levels for H_0 of 5.5% and 3.4% for 10,000 and 20,000 injections, respectively, in agreement with the Fisher matrix estimations.

In the previous analysis we assumed that one hyperparameter is enough to model our ignorance on the source distribution. In the Appendix A we show that one more hyperparameter can capture a possible bias in the adopted start formation rate model. This prevents the introduction of a bias in the Hubble constant at the price of degrading the precision of its determination, which worsen by a factor ≈ 2 .

⁴ pypi.org/project/numdifftools.

# injs	σ_{H_0}/H_0	
	$[\sigma_{d_L}/d_L = 5\%]$	$[\sigma_{d_L}/d_L = 10\%]$
10,000	4.9%	12.1%
20,000	3.0%	7.6%
40,000	2.7%	6.5%

Table 2. Forecasted relative constraints on H_0 for third-generation gravitational-wave detectors.

# injs	$\left[\langle (H_{0,\text{inj}}/H_{0,\text{rec}} - 1)^2 \rangle\right]^{1/2}$	
	$[\sigma_{d_L}/d_L = 5\%]$	$[\sigma_{d_L}/d_L = 10\%]$
10,000	2.7%	3.3%
20,000	1.0%	1.0%
40,000	0.5%	0.9%

Table 3. Forecasted bias on H_0 for third-generation gravitational-wave detectors.

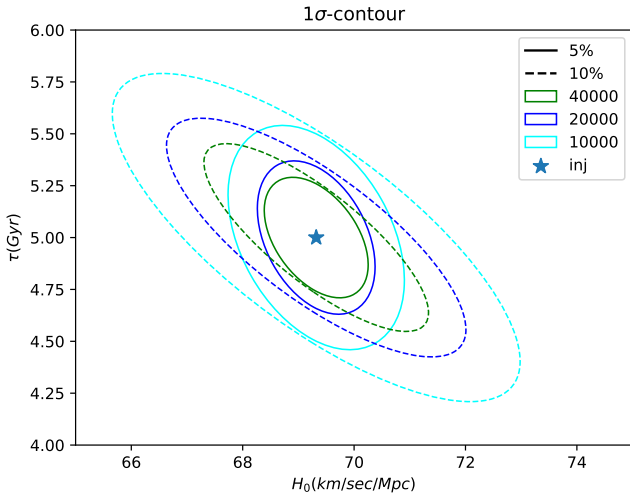


Figure 9. 1σ covariance regions from averaged Fisher matrix.

5 CONCLUSIONS

Detections of gravitational waves from binary coalescences have opened new ways to investigate cosmology. In particular, while using concurrent observations of redshift and luminosity distance is an obvious way to measure the Hubble constant, data from the first three observation runs of LIGO and Virgo showed that binary black holes, dark sirens without an electromagnetic counterpart, are far more frequent than neutron star binaries with electromagnetic counterpart. Note, however, that forecasts for third generation detectors indicate that one could constrain the Hubble constant to sub-percent level by accumulating electromagnetically bright standard sirens over 10 years at a rate of ~ 30 bright standard sirens per year (Belgacem et al. 2019).

On the other hand, by exploiting the gravitationally measured source location, in the case of a network of at least three detectors, it has been shown that already with $O(200)$

dark siren events one can achieve a few percent measurement of H_0 if the galaxy catalogs are at least 25% complete (Gray et al. 2020). This can be assumed only for relatively close sources, although galaxy catalogs complete to magnitude 24 are expected to be produced by Euclid (Blanchard et al. 2020), allowing to see a milky way-type galaxy up to 1 Gpc.

Here, we proposed an independent method, where redshift information comes from our partial knowledge of the source distribution. Marginalizing over the hyper-parameter encoding our ignorance of the binary astrophysical distributions we can estimate the Hubble constant with a few percent precision with few tens of thousands black siren detections, without the need of multiple detectors, galaxy catalogs or electromagnetic counterparts to have information about the individual source redshifts. Note that, while the forecasted rate of binary black hole coalescence detections by third generation gravitational wave observatories is subject to large uncertainties, even in the more pessimistic scenarios few $O(10^3)$ detections per month should be made so that our method should be a viable alternative.

There are, however, caveats in our method. First, to take into account detector-related selection effects, we have simulated future detections with a specific black hole mass function. This will be addressed by the time our method will be used. Indeed, 3G detectors will have accumulated tens of thousands of BBH detections so that we expect such mass function to be known accurately. Second, the star formation rate we assumed may not correspond to the one realized in nature and the model we presented in the main text, with only one hyperparameter, may be an oversimplification. To test these assumptions we have performed simulations in which data was injected and analyzed using different star formation rate models. The results reported in the Appendix A show that the addition of an another hyperparameter can capture the difference in underlying star formation rate model and prevent the introduction of a bias in the Hubble constant, though degrading the precision of its determination.

ACKNOWLEDGEMENTS

The work of HL is financed in part by the Coordenação de Aperfeiçoamento de Pessoal de Nível Superior - Brasil (CAPES) – Finance Code 001. VM thanks CNPq and FAPES for partial financial support. RS thanks CNPq for partial financial support under grant n. 312320/2018-3. This project has received funding from the European Union’s Horizon 2020 research and innovation programme under the Marie Skłodowska-Curie grant agreement No 888258. We thank the High Performance Computing Center (NPAD) at UFRN for providing computational resources.

REFERENCES

- Aasi J., et al., 2015, *Class. Quant. Grav.*, 32, 074001, [1411.4547].
- Abbott B. P., et al., 2017a, *Class. Quant. Grav.*, 34, 044001, [1607.08697].
- Abbott B., et al., 2017b, *Nature*, 551, 85, [1710.05835].
- Abbott B. P., et al., 2019, *Astrophys. J. Lett.*, 882, L24, [1811.12940].
- Abbott B. P., et al., 2020, *Living Rev. Rel.*, 23, 3.

Abbott B. P., et al., 2021a, *Astrophys. J.*, 909, 218, [1908.06060].

Abbott R., et al., 2021b, *Astrophys. J. Lett.*, 913, L7, [2010.14533].

Acernese F., et al., 2015, *Class. Quant. Grav.*, 32, 024001, [1408.3978].

Aghanim N., et al., 2020, *Astron. Astrophys.*, 641, A6, [1807.06209].

Akutsu T., et al., 2020, [2005.05574].

Ashton G., et al., 2019, *Astrophys. J. Suppl.*, 241, 27, [1811.02042].

Belgacem E., Dirian Y., Foffa S., Howell E. J., Maggiore M., Regimbau T., 2019, *JCAP*, 08, 015, [1907.01487].

Blanchard A., et al., 2020, *Astron. Astrophys.*, 642, A191, [1910.09273].

Camarena D., Marra V., 2018, *Phys. Rev.*, D98, 023537, [1805.09900].

Camarena D., Marra V., 2021, *Mon. Not. Roy. Astron. Soc.*, in press, [2101.08641].

Chen H.-Y., Fishbach M., Holz D. E., 2018, *Nature*, 562, 545, [1712.06531].

Dalal N., Holz D. E., Hughes S. A., Jain B., 2006, *Phys. Rev. D*, 74, 063006, [astro-ph/0601275].

Del Pozzo W., 2012, *Phys. Rev.*, D86, 043011, [1108.1317].

Di Valentino E., et al., 2021, *Class. Quant. Grav.*, 38, 153001, [2103.01183].

Diaz C. C., Mukherjee S., 2021, [2107.12787].

Ding X., Biesiada M., Zheng X., Liao K., Li Z., Zhu Z.-H., 2019, *JCAP*, 04, 033, [1801.05073].

Ezquiaga J. M., Holz D. E., 2021, *Astrophys. J. Lett.*, 909, L23, [2006.02211].

Farr W. M., Fishbach M., Ye J., Holz D., 2019, *Astrophys. J. Lett.*, 883, L42, [1908.09084].

Fishbach M., et al., 2019, *Astrophys. J. Lett.*, 871, L13, [1807.05667].

Foreman-Mackey D., Hogg D. W., Lang D., Goodman J., 2013, *Publ. Astron. Soc. Pac.*, 125, 306, [1202.3665].

Gray R., et al., 2020, *Phys. Rev. D*, 101, 122001, [1908.06050].

Hall E. D., Evans M., 2019, *Class. Quant. Grav.*, 36, 225002, [1902.09485].

Heger A., Fryer C., Woosley S., Langer N., Hartmann D., 2003, *Astrophys. J.*, 591, 288, [astro-ph/0212469].

Holz D. E., Hughes S. A., 2005, *Astrophys. J.*, 629, 15, [astro-ph/0504616].

Husa S., Khan S., Hannam M., Pürrer M., Ohme F., Jiménez Forteza X., Bohé A., 2016, *Phys. Rev. D*, 93, 044006, [1508.07250].

Khan S., Husa S., Hannam M., Ohme F., Pürrer M., Jiménez Forteza X., Bohé A., 2016, *Phys. Rev. D*, 93, 044007, [1508.07253].

Khetan N., et al., 2021, *Astron. Astrophys.*, 647, A72, [2008.07754].

Knox L., Millea M., 2020, *Phys. Rev. D*, 101, 043533, [1908.03663].

LIGO Scientific Collaboration 2018, LIGO Algorithm Library - LALSuite, free software (GPL), doi:10.7935/GT1W-FZ16

Lewis A., 2019, [1910.13970].

Madau P., Dickinson M., 2014, *Ann. Rev. Astron. Astrophys.*, 52, 415, [1403.0007].

Mastrogiovanni S., et al., 2021, [2103.14663].

Messenger C., Read J., 2012, *Phys. Rev. Lett.*, 108, 091101, [1107.5725].

Mukherjee S., Wandelt B. D., 2018, [1808.06615].

Mukherjee S., Wandelt B. D., Nissanke S. M., Silvestri A., 2021a, *Phys. Rev. D*, 103, 043520, [2007.02943].

Mukherjee S., Wandelt B. D., Silk J., 2021b, *Mon. Not. Roy. Astron. Soc.*, 502, 1136, [2012.15316].

Nissanke S., Holz D. E., Hughes S. A., Dalal N., Sievers J. L., 2010, *Astrophys. J.*, 725, 496, [0904.1017].

Perivolaropoulos L., Skara F., 2021, [2105.05208].

Punturo M., et al., 2010, *Class. Quant. Grav.*, 27, 194002.

Riess A. G., Casertano S., Yuan W., Bowers J. B., Macri L.,

Zinn J. C., Scolnic D., 2021, *Astrophys. J. Lett.*, 908, L6, [2012.08534].

Robertson B. E., Ellis R. S., 2012, *ApJ*, 744, 95, [1109.0990].

Schutz B. F., 1986, *Nature*, 323, 310.

Scolnic D. M., et al., 2018, *Astrophys. J.*, 859, 101, [1710.00845].

Soares De Souza J. M., Sturani R., 2021, *Phys. Dark Univ.*, 32, 100830, [1905.03848].

Soares-Santos M., et al., 2019, *Astrophys. J.*, 876, L7, [1901.01540].

Verde L., Treu T., Riess A., 2019, [1907.10625], doi:10.1038/s41550-019-0902-0

Vitale S., Farr W. M., Ng K., Rodriguez C. L., 2019, *Astrophys. J. Lett.*, 886, L1, [1808.00901].

Ye C., Fishbach M., 2021, *Phys. Rev. D*, 104, 043507, [2103.14038].

You Z.-Q., Zhu X.-J., Ashton G., Thrane E., Zhu Z.-H., 2021, *Astrophys. J.*, 908, 215, [2004.00036].

Zhu L.-G., Hu Y.-M., Wang H.-T., Zhang J.-D., Li X.-D., Hendry M., Mei J., 2021, [2104.11956].

APPENDIX A: ROBUSTNESS AGAINST UNKNOWN STAR FORMATION RATE

Our analysis adopts the star formation rate density ψ_{MD14} of equation (14) from Madau & Dickinson (2014). Here, we investigate the impact of analyzing with ψ_{MD14} data that were produced with the alternative star formation rate density by Robertson & Ellis (2012):

$$\psi_{\text{RE12}}(z) = \left[\frac{0.007 + 0.27(z/3.7)^{2.5}}{1 + (z/3.7)^{6.4}} + 0.003 \right] M_{\odot} \text{ yr}^{-1} \text{ Mpc}^{-3}, \quad (\text{A1})$$

to have a proxy of the bias we may introduce in the cosmological parameter estimation by adopting an incorrect underlying star formation and merger distribution. Both functions are plotted in Fig. A1. Fig. A2 shows that despite the two underlying star formation rates are qualitatively different, the resulting merger rates can be made to overlap by adjusting the C parameter of Eq. (14), which we now promote to hyperparameter (and treat as a nuisance parameter).

We then show in Fig. A3 the results of an analysis in which the probability distributions for H_0 , Ω_m and the two nuisance parameters τ and C are obtained in the case in which the injections are generated assuming the star formation rate (A1) but analyzed with the star formation rate (14). One can see that the hyperparameter C , by taking a value different from the original one of eq. (14), absorbs the effect of a different star formation rate, avoiding a bias in H_0 . On the other hand, the precision on H_0 is degraded to almost 10% percent level, thus requiring several tens of thousand of injections to reach percent level.

This paper has been typeset from a \LaTeX file prepared by the author.

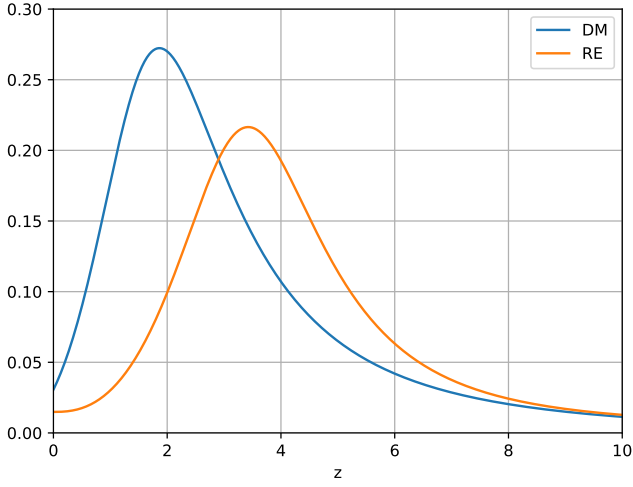


Figure A1. The star formation rate of eqs. (14) and (A1).

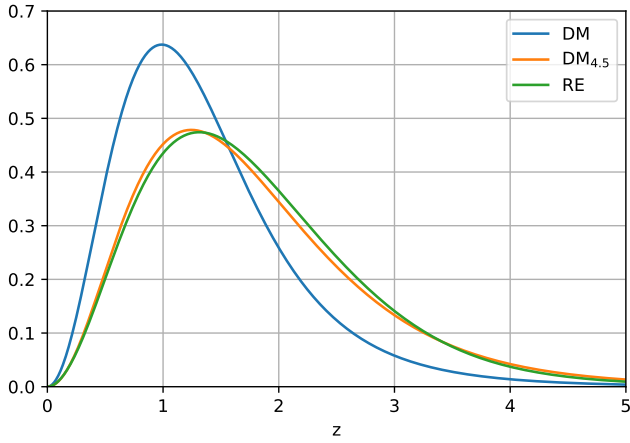


Figure A2. Comparison of normalized detected merger rate assuming the DM star formation rate (14), the RE one (A1), or the one of eq. (14) with $C = 4.5$.

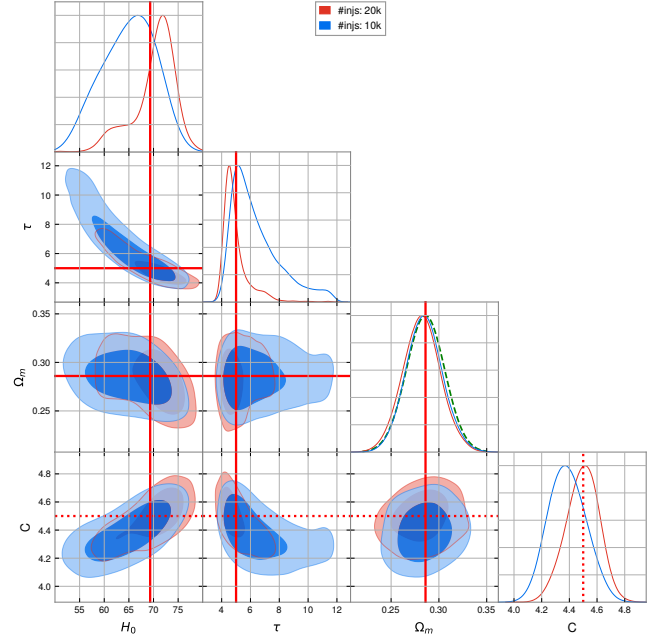


Figure A3. Statistical inference for injections generated according to the star formation rate of Eq. (A1) but analyzed using the star formation rate of Eq. (14), for 5% relative errors in the measurement of d_L , with 20,000 and 10,000 injections. Here, the model includes the nuisance parameter C , which absorbs the effect of a different star formation rate between injection and recovery, with the result of keeping H_0 unbiased.